Transmission and Reflection Diffraction Tomography in Breast Imaging

Francesco Simonetti

Department of Mechanical Engineering, Imperial College,
London SW7 2AZ, United Kingdom
f.simonetti@imperial.ac.uk

Lianjie Huang

MS D443, Los Alamos National Laboratory
Los Alamos, NM 87545, USA
ljh@lanl.gov

Neb Duric

Karmanos Cancer Institute, Wayne State University
4100 John R, Detroit, Michigan 48201, USA
duric@karmanos.org

Abstract

Commercial medical ultrasound scanners produce images of human tissue by interpreting the information carried by echoes reflected from structures contained inside it. In this paper, a new generation of toroidal ultrasound arrays is used to measure both the signals reflected and transmitted through the tissue. It is shown that transmission measurements encode complete information about the gross structure of the tissue and lead to images that are superior to those obtained form reflection measurements alone. Experimental results are provided for a gel phantom and a human breast in vivo.

1. Introduction

Since the 1970s, researchers have been investigating the possibility of using ultrasound for the diagnosis of breast cancer [6, 7, 4]. Although it is not yet used in medical diagnostics, ultrasound tomography could offer a number of advantages over the gold standard of X-ray mammography which include: earlier diagnosis [8], absence of ionizing radiation, and lower cost.

One of the problems encountered in conventional sonography is the characteristic granular appearance of sonograms caused by the speckle phenomenon. In commercial scanners, this is caused by beamforming, which leads to complex interference patterns that result from the coherent nature of ultrasound [1]. Although speckle contrast is used to separate different features within an image, the appearance of speckle can also mask small abnormalities. In this context, several authors have observed that computerized ultrasound tomography (CUT) leads to speckle-free images [4, 5]. CUT uses ultrasound transmitted through the

tissue and is based on the ray approximation of geometrical optics. Because of this approximation, interference, which is the very causes for the appearance of speckle in coherent imaging, is neglected, resulting in the suppression of speckle. However, the ray approximation is known to cause resolution degradation and image artifacts due to its inability to account for diffraction [15]. Therefore, it is largely accepted that reflection and CUT images complement each other since the first provides high-resolution information about the boundaries of regions of sudden impedance variations, whereas, the latter provides quantitative information about the impedance distribution [4].

Recently, several research groups have been investigating the potential of imaging methods that can account for diffraction [2, 9, 14] or even multiple scattering [12]. These works employ toroidal arrays of transreceivers that surround the tissue and enable its insonification from any direction in the plane of the array. For each insonification, both the backscattered and transmitted fields are measured simultaneously (prototype toroidal arrays with as many as 1024 [2] or more recently 2048 [13] transreceivers have been manufactured). However, these studies have not investigated the extent to which backscattering and through transmission provide information about the tissue properties and if they complement each other.

This paper addresses these questions in the framework of diffraction tomography. Images obtained with reflection and transmission diffraction tomography are compared for the cases of continuous-wave (CW) and broadband excitation. Section 2 reviews the main aspects of the theory of diffraction tomography and links reflection and transmission imaging. Section 3 presents two sets of experiments performed with a gel phantom and a human breast *in vivo*. The gel phantom is well characterized and can be used to assess the information revealed by the reflection and trans-
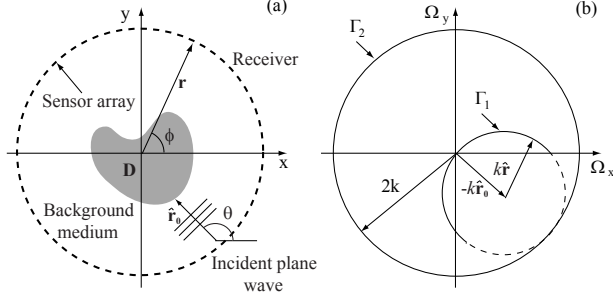
IEEE
computer
society

Figure 1. (a) Diagram of a toroidal array used in ultrasound tomography. (b) Two dimensional K-space showing how the scattered field measured in the direction $\hat{\mathbf{r}}$ and due to an incident plane wave from direction $\hat{\mathbf{r}}_0$ maps onto the point $\Omega = 2\pi/\lambda(\hat{\mathbf{r}}_0 - \hat{\mathbf{r}})$ of the K-space.

mission images. On the other hand, the breast sample which has a more uncertain anatomy, is used to give a qualitative assessment of the performance of the two approaches when they are applied to the actual tissue.

2. Reflection and transmission diffraction tomography

The objective of diffraction tomography is to reconstruct the spatial distribution of a target material property, defined by the object function [1] $O(\mathbf{r})$, from the perturbation induced by the object's structure on the free propagation of ultrasound. Central to this is the existence of a one-to-one mapping between the perturbation, p, and the spatial Fourier transform of the object function, O, which defines the so-called K-space,

$$p \longleftrightarrow O. \qquad (1)$$

The definition of the perturbation in eq. (1) depends on the model used to describe the interaction between the incident wave and the probed object. To illustrate this, let us consider the two-dimensional scattering problem depicted in Fig. 1(a) whereby a monochromatic plane wave propagating in the direction $\mathbf{r}_0$ is incident on an object of support D. Assuming that the scattering problem can be expressed by a scalar potential, the field detected by an array sensor placed in the far field at position $\mathbf{r}$, $\psi(\mathbf{r}, k\hat{\mathbf{r}}_0)$, is given by

$$\lim_{r\to\infty} \psi(\mathbf{r}, k\hat{\mathbf{r}}_0) = \exp\left(ik\hat{\mathbf{r}}_0 \cdot \mathbf{r}\right) + f(k\hat{\mathbf{r}}, k\hat{\mathbf{r}}_0)\frac{\exp\left(ikr\right)}{\sqrt{r}}, \quad (2)$$

---

[1]The object function is relate to the index of refraction map, $n(\mathbf{r})$, via the relationship $O(\mathbf{r}) = k^2[n(\mathbf{r})^2 - 1]$

where the first term of the right hand side is the incident plane wave, which propagates with wavelength λ ($k = 2\pi/\lambda$) and $f(k\hat{\mathbf{r}}, k\hat{\mathbf{r}}_0)$ is the scattering amplitude defined as

$$f(k\hat{\mathbf{r}}, k\hat{\mathbf{r}}_0) = \Pi \int_D d^2r' \exp(-ik\hat{\mathbf{r}}\cdot\mathbf{r}')O(\mathbf{r}')\psi(\mathbf{r}', k\hat{\mathbf{r}}_0), \quad (3)$$

with

$$\Pi = \frac{\exp(i\pi/4)}{\sqrt{8\pi k}}. \qquad (4)$$

It can be shown that under the Born approximation, the perturbation p in eq. (1) coincides with the scattering amplitude [3]

$$p(k\hat{\mathbf{r}}, k\hat{\mathbf{r}}_0) = f(k\hat{\mathbf{r}}, k\hat{\mathbf{r}}_0) = \Pi O[k(\hat{\mathbf{r}} - \hat{\mathbf{r}}_0)]. \qquad (5)$$

This relationship links the measurements to the Fourier transform of the object function, $O(\Omega)$, directly. In fact, the scattering amplitude can be measured experimentally with a toroidal array of transreceivers, by transmitting with each sensor sequentially and detecting the total field with all the sensors in parallel. The scattered field is then obtained by subtracting the incident field, measured before placing the object within the array, from the total field. The diagram in Fig. 1 shows how a particular transmit and receive pair maps onto a point of the K-space. In particular, for a given transmitter position defined by $\hat{\mathbf{r}}_0$ the measurements map onto the circle Γ_1 as the receiver direction, $\hat{\mathbf{r}}$, spans the entire array. This is known as the Ewald circle. The solid part of the circle corresponds to the so-called transmission measurements (the angle between $\hat{\mathbf{r}}$ and $\hat{\mathbf{r}}_0$ is less than $\pi/2$) whereas, the dashed part corresponds to the backscattering measurements. As the position of the transmitter revolves around the object, the Ewald circle sweeps a disk of the K-space with radius $2k$ known as the Ewald Limiting Disk (ELD) and labeled as Γ_2 in Fig. 1(b).

From the knowledge of $O(\Omega)$ within the ELD, $O(\mathbf{r})$ can be reconstructed by assuming that $O(\Omega)$ vanishes outside the ELD and performing the inverse Fourier transform. This leads to a low pass filtered image of the object function, I_{DT}, which in the K-space is given by

$$I_{DT}(\Omega) = O(\Omega)H_{DT}(\Omega), \qquad (6)$$

with

$$H_{DT}(\Omega) = \begin{cases} 1 & |\Omega| < 2k \\ 0 & |\Omega| > 2k. \end{cases} \qquad (7)$$

Physically this means that only the characteristics of the object that vary on a spatial scale longer than $\lambda/2$ can be reconstructed and leads to the classical diffraction limit.
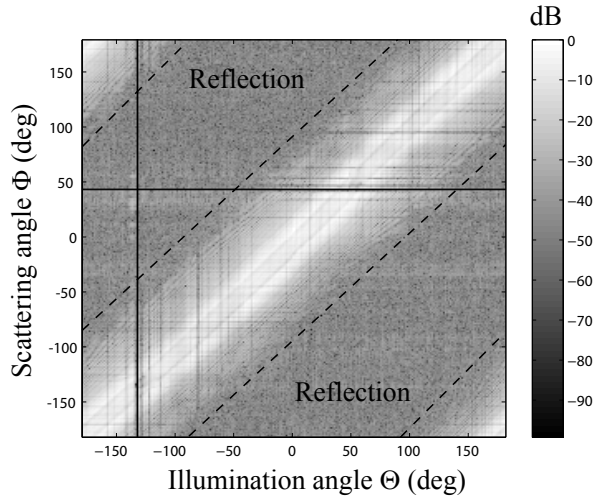
Figure 2. Modulus of the scattering amplitude at 1.2MHz as a function of the illumination angle Θ and the scattering angle Φ.

In transmission tomography, the object function is reconstructed from only the transmission measurements. Therefore, as the transmitter revolves around the object the half solid circle in Fig. 1(b) describes a disk of radius $\sqrt{2}k$ centered at the origin and contained within the ELD. In other words, transmission tomography provides a low pass filtered image with cutoff $\sqrt{2}k$ rather than $2k$. A similar argument shows that reflection tomography provides a band pass filtered image of the object with cutoffs at $\sqrt{2}k$ and $2k$.

This analysis suggests that reflection tomography complements transmission tomography by reconstructing the spatial frequencies between $\sqrt{2}k$ and $2k$.

3. Experiments

Two sets of experiments were performed with a 256 element ultrasonic array developed at Karmanos Cancer Institute [5, 12]. The tests were carried out with a gel phantom and a human breast *in vivo* using the setup depicted in the diagram of Fig. 1(a). Both the array and the specimen where immersed in a water bath.

3.1. Gel phantom

This specimen consisted of a water based gel cylinder 35mm diameter with a hole in the center 5mm diameter. The hole was filled with cold water so as to produce an inclusion with low speed of sound. The temperature of the water bath was 25.7C^o. Figure 2 shows the modulus of the

scattering amplitude at 1.2MHz as a function of the insonification direction Θ and the scattering angle Φ. The color scale is in dB and represents the modulus normalized with respect to the largest measurement. The bright central diagonal that extends towards the two dashed lines corresponds to the transmission measurements along with the two triangular bands on the top left and bottom right corners. The backscattering measurements correspond to the two remaining reflection bands. Details about the calculation of the scattering amplitude are given in [12].

The transmission measurements reveal the presence of clear patterns, which are related to the phantom (bright curves). On the other hand, the reflection measurements are randomly distributed meaning that they bring little information about the phantom as confirmed by the images in Fig. 3. In particular, Fig. 3(a) is the diffraction tomography image of the phantom at 1.2MHz obtained by con-
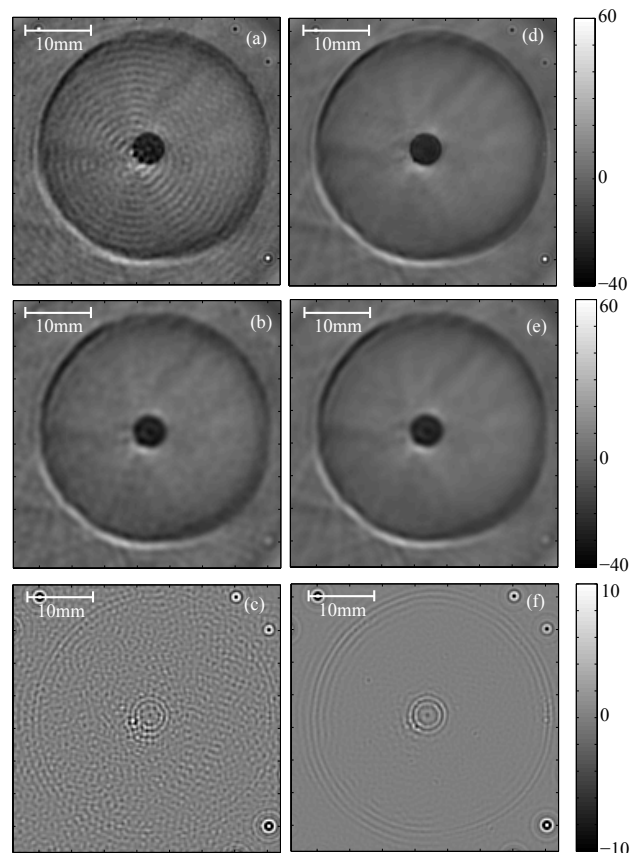

Figure 3. (a)-(c) CW images of the phantom at 1.2MHz. (d)-(f) broadband (1.1-1.3MHz) images. (a) and (d) diffraction tomography; (b) and (e) transmission tomography; (c) and (f) reflection tomography.
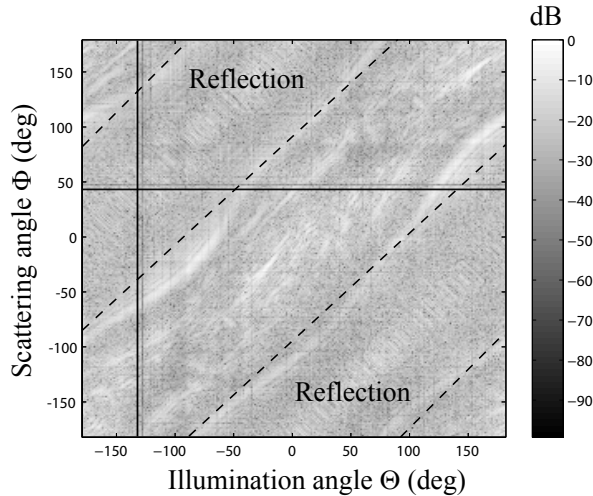
Figure 4. Modulus of the scattering amplitude at 1.2MHz measured for a breast *in vivo***.**

sidering both the reflection and transmission data in Fig. 2, details about the algorithm used to calculate the image can be found in [10]. The color scale shows the difference between the reconstructed velocity map and the velocity of the water background in m/s. Next, Figs 3(b) and (c) are the images obtained with transmission and reflection data only. As expected, the transmission image reproduces all the features of the phantom and is similar to the image in Fig. 3(a). In contrast, the reflection image provides a low resolution and noisy reconstruction; the boundaries of the phantom are barely visible and the values of velocity are incorrect. Figures 3(d)-(f) show the broadband versions of the images in Figs 3(a)-(c) reconstructed over the bandwidth 1.1-1.3MHz. While the transmission image does not benefit from the broadband excitation significantly [Figs 3(b) and (e)], the broadband reflection image contains a lower level of noise than the CW image [Figs 3(c) and (f)]. Over all, the transmission image is superior to the reflection image in terms of resolution and estimation of the sound-speed map.

3.2. Human breast *in vivo*

This set of experiments was carried out with a patient lying on a bed with her breast suspended within the array through a circular aperture in the bed [5]. Figure 4 shows the modulus of the scattering amplitude measured for the breast. As in the case of the gel phantom, the reflection measurements do not reveal any pattern that could be associated with the breast. In contrast, the transmission measurements encode a large amount of information about the complex internal structure of the breast. This information is displayed in Fig. 5(a) which is a CW transmission im-

age of a coronal slice of the breast at 750kHz obtained from the measurements in Fig. 4. The image shows the skin of the breast and a complex network of fibrous structures in the central part of the breast which could correspond to the ducts or Cooper's ligaments. The dashed circle indicates a region containing a tumor diagnosed with X-ray mammography and conventional ultrasound. Next, Fig. 5(b) is the CW reflection image. This is biased by noise and does not bear information about the breast anatomy. Figures 5(c) and (d) are the broadband transmission and reflection images, respectively. Although the bandwidth was 100kHz only a dramatic improvement can be observed in the case of the reflection image, Fig. 5(d), which now reveals the skin of the breast and some of the internal structures. However, as in the case of the gel phantom, the reflection image does not contain any additional information compared to the transmission image.

Lastly, it should be observed that the transmission image in Fig. 5(c) is relatively free of speckle compared to the reflection image in Fig. 5(d). The physical mechanism that leads to the speckle reduction in Fig. 5(c), which is a coherent image, is different from that associated with CUT. In fact, the acoustic signature of the fine structure of the breast, which would cause the speckle, is encoded in the ballistic transmitted wave which after emerging from the breast is
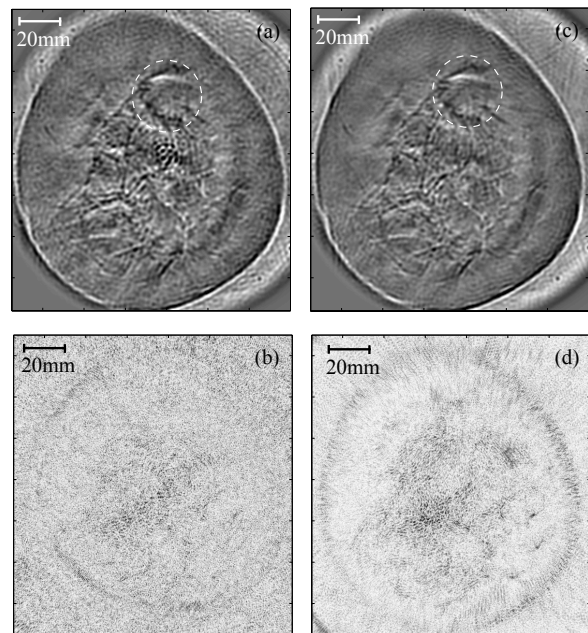

Figure 5. Images of a human breast *in vivo***. (a) and (b) CW transmission and reflection images; (c) and (d) broadband transmission and reflection images.**

deflected away from the receivers [11].

4. Conclusions

This paper has investigated the use of reflection and transmission diffraction tomography in breast imaging. It is largely accepted that reflection imaging complements computerized ultrasound tomography (CUT), because it provides better reconstructions of the boundaries where acoustic impedance discontinuities occur.

The experiments reported in this paper for a gel phantom and a human breast *in vivo* suggest that reflection imaging does not provide additional information compared to transmission diffraction tomography. This is contrast with the theory of diffraction tomography which predicts that the reflection images should contain higher spatial frequencies than transmission ones. Instead, the measurement have shown that the backscattering is weak and buried in the background noise.

Finally, reflection tomography exhibits a greater sensitivity to the bandwidth of the excitation than transmission tomography. While narrowband excitation can lead to high quality images in transmission tomography, reflection tomography requires the use of wideband signals.

References

[1] J. G. Abbott and F. L. Thurstone. Acoustic speckle: theory and experimental analysis. *Ultrason. Imag.*, 1:303–324, 1979.

[2] M. P. Andre, M. P. Janee, H. S., G. P. Otto, B. A. Spivey, and P. D. A. High-speed data acquisition in a diffraction tomography system employing large-scale toroidal arrays. *Int. J. Imag. Syst. Tech.*, 8:137–147, 1997.

[3] M. Born and E. Wolf. *Principles of Optics*. Cambridge University Press, Cambridge, 1999.

[4] P. L. Carson, C. R. Meyer, A. L. Scherzinger, and T. V. Oughton. Breast imaging in coronal planes with simultaneous pulse echo and transmission ultrasound. *Science*, 214(4):1141–1143, 1981.

[5] N. Duric, L. Littrup, P. Poulo, A. Babkin, R. Pevzner, E. Holsapple, O. Rama, and C. Glide. Detection of breast cancer with ultrasound tomography: First results with the computed ultrasound risk evaluation (cure) prototype. *Med. Phys.*, 34(2):773–785, 2007.

[6] J. F. Greenleaf, S. A. Johnson, S. L. Lee, G. T. Herman, and E. H. Wood. Algebraic reconstruction of spatial distributions of acoustic absorption within tissue from their two-dimensional acoustic projections. In P. S. Green, editor, *Acoustical Holography*, volume 5, pages 591–603. Plenum Press, New York, 1973.

[7] J. F. Greenleaf, S. A. Johnson, W. F. Samayoa, and F. A. Duck. Algebraic reconstruction of spatial distributions of acoustic velocities in tissue from their time-of-flight profiles. In P. S. Green, editor, *Acoustical Holography*, volume 6, pages 71–90. Plenum Press, New York, 1975.

[8] T. M. Kolb, J. Lichy, and J. H. Newhouse. Comparison of the performance of screening mammography, physical examination, and breast us and evaluation of factors that influence them: An analysis of 27,825 patient evaluation. *Radiology*, 225:165–175, 2002.

[9] F. Lin, A. I. Nachman, and R. C. Waag. Quantitative imaging using a time-domain eigenfunction method. *J. Acoust. Soc. Am.*, 108(3):899–912, 2000.

[10] F. Simonetti and Huang. From beamforming to diffraction tomography. *J. Appl. Phys.*, Submitted, 2007.

[11] F. Simonetti, L. Huang, and N. Duric. High-resolution ultrasound tomography of complex three-dimensional objects. *submitted for publication*, 2007.

[12] F. Simonetti, L. Huang, N. Duric, and O. Rama. Imaging beyond the born approximation: An experimental investigation with an ultrasonic ring array. *Phys. Rev. E*, 76:036601, 2007.

[13] R. C. Waag and R. J. Fedewa. A ring transducer system for medical ultrasound research. *IEEE Trans. Ultrason. Ferroelectr. Freq. Control*, 53(10):1707–1718, 2006.

[14] R. C. Waag, F. Lin, T. K. Varslot, and J. P. Astheimer. An eigenfunction method for reconstruction of large-scale and high-contrast objects. *IEEE Trans. Ultrason. Ferroelectr. Freq. Control*, 54(7):1316–1332, 2007.

[15] P. R. Williamson and M. H. Worthington. Resolution limits in ray tomography due to wave behavior: Numerical experiments. *Geophysics*, 58(5):727–735, 1993.